Solar Neutrino Flux Measurement from the Pure D_2O-Phase of the Sudbury Neutrino Observatory

Y. Chan[a*] for the SNO Collaboration [1]

[a]Institute for Nuclear and Particle Astrophysics, Nuclear Science Division, Lawrence Berkeley National Laboratory, Berkeley, California 94720, U.S.A.

The measured ν_e component of the solar neutrino flux from the pure-D_2O phase (at 5 MeV threshold) is $\phi_e = 1.76^{+0.06}_{-0.05}(\text{stat.})^{+0.09}_{-0.09}$ (syst.) $\times 10^6$ cm^{-2}s^{-1} and the non-ν_e component $\phi_{\mu\tau} = 3.41^{+0.45}_{-0.45}(\text{stat.})^{+0.48}_{-0.45}$ (syst.) $\times 10^6$ cm^{-2}s^{-1}, 5.3σ greater than zero. This provides a strong model independent evidence for solar ν_e flavor transformation. The measured total flux, $\phi_{NC} = 5.09^{+0.44}_{-0.43}(\text{stat.})^{+0.46}_{-0.43}$ (syst.) $\times 10^6$ cm^{-2}s^{-1}, is consistent with solar models. A day-night asymmetry study has also been performed. When combined with other measurements, the LMA region of the MSW parameter space is strongly favored.

1. Introduction

The Sudbury Neutrino Observatory [2](SNO) is an underground heavy water Cherenkov detector located at a depth of 6010 m of water equivalent in Sudbury, Ontario, Canada. SNO is capable of providing a definitive and model *independent* solution to the solar neutrino problem by performing both charged-current (CC, sensitive to ν_e only) and neutral-current (NC, equally sensitive to all active neutrinos) measurements of the solar neutrino flux. If there is no ν_e flavor transformation the CC/NC ratio should equal to unity and vice versa. The basic idea and method have been outlined in 1980 by H. Chen [3]. As a real-time detector, SNO can also measure the solar ^8B neutrino energy spectrum and temporal variations of the solar neutrino flux, providing additional model independent information.

Table 1 summarizes the three SNO neutrino reactions that take place in the D_2O region of the detector. Since the neutral current (NC) interaction has *equal* sensitivity to all active neutrinos it is a powerful tool for measuring the *total* active solar neutrino flux. The signature for the NC interaction is a free neutron. In the pure D_2O phase, the neutron can be recaptured in D_2O releasing a mono-energetic γ-ray :

$$D_2O \text{ phase } NC : n + d \rightarrow t + \gamma \ (6.25MeV) \tag{1}$$

and be detected.

*Supported by DOE Contract No. DE-AC03-76SF00098

Table 1
Comparison of SNO reactions for active neutrinos and the 3 NC detection methods.

Type	**SNO Active Neutrino Reactions**		
	Charged-Current (CC)	**Neutral Current (NC)**	**Elastic Scattering (ES)**
ν_e	ν_e+d $\rightarrow e^-$+p+p 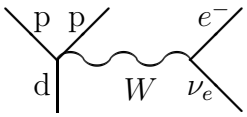	ν_e+d $\rightarrow \nu_e$+p+n 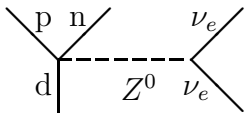	$\nu_e+e^- \rightarrow \nu_e+e^-$ 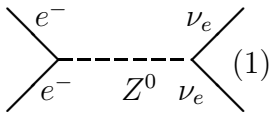 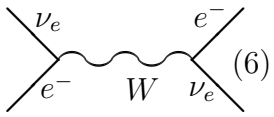
$\nu_{\mu,\tau}$	n/a	$\nu_{\mu,\tau}$+d $\rightarrow \nu_{\mu,\tau}$+p+n 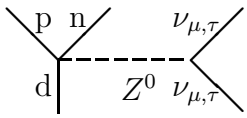	$\nu_{\mu,\tau}+e^- \rightarrow \nu_{\mu,\tau}+e^-$ 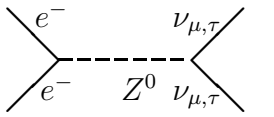
Q-Value	1.4 MeV	2.2 MeV	0
Event Direction	Backward-peaked (1-0.340cos $\theta_\odot$)	None	Forward-peaked wrt $\theta_\odot$
Region	D_2O only	D_2O only	D_2O + H_2O
Spectral	Yes	No	Yes
Rate/Flux	Yes	Yes	Yes
Primary backgrounds	β, γ radioactivity	d(γ,n)p ($E_\gamma \geq 2.2$ MeV) and spallation n	β, γ radioactivity
D_2O Phase Detection	e^- Cherenkov	d(n,γ)t 6.25 MeV	e^- Cherenkov
Salt Phase Detection	e^- Cherenkov	$^{35}Cl(n,\gamma)^{36}Cl$ 8.6 MeV Cascade	e^- Cherenkov
NCD Phase Detection	e^- Cherenkov	NCD $^3He(n,p)t$ 764 keV	e^- Cherenkov

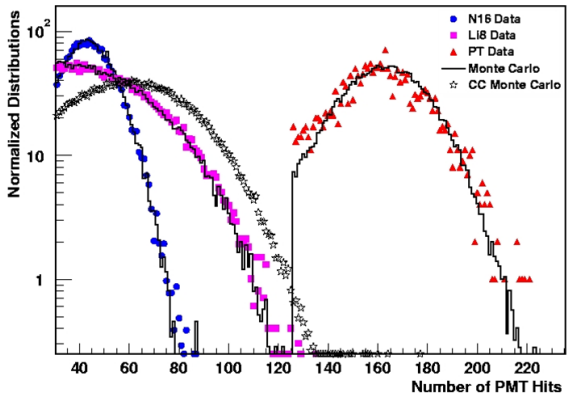

Figure 1. Comparison of calibration source data and SNO Monte Carlo. Also shown is a Monte Carlo signal CC spectrum. It can be seen that the solar neutrino energy range is well covered by the calibration sources deployed.

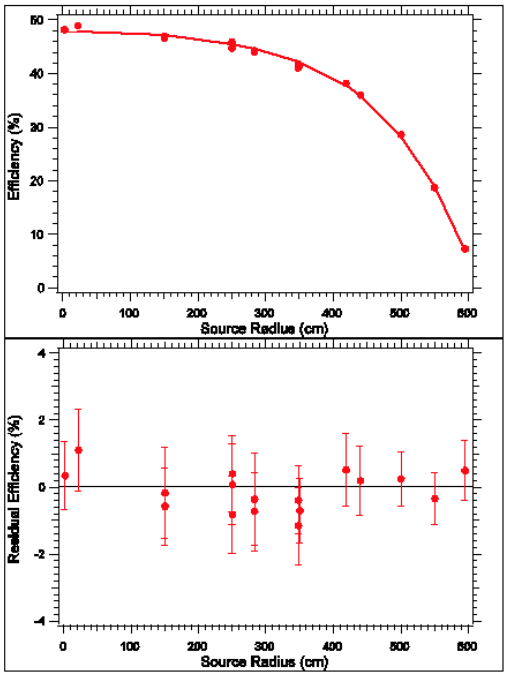

Figure 2. Neutron capture efficiency determined from the ^{252}Cf source.

2. Detector Calibration

Since SNO is a complex detector made up of a large number of components, extensive calibration is needed in order to characterize the detector's optical and energy responses (see Table 2). The absolute energy scale, position dependence, and uncertainties are established with a collection of radioactive sources including a tagged ^{16}N source deployed over two planar grids within the D_2O and a linear grid in the H_2O. The neutron response of the detector was calibrated with a ^{252}Cf source (Figure 2). The deduced efficiency for neutron captures on deuterium is $29.9 \pm 1.1\%$ for a uniform source of neutrons in the D_2O. The neutron detection efficiency within the fiducial volume and above the energy threshold is 14.4%.

Figure 1 shows a comparison of the different calibration source data with Monte Carlo simulations. The agreement is very good and the deduced energy scale uncertainty is $\approx$1.2%. The vertex reconstruction accuracy and resolution are measured using Compton electrons from the ^{16}N source, and the energy and source variation of reconstruction are checked with a ^{8}Li β source. Angular resolution is measured using Compton electrons produced more than 150 cm from the ^{16}N source. At these energies, the vertex resolution

Table 2
Partial list of calibration sources deployed during the pure D_2O phase.

Calibration	Range	Source
Optics	337 -620 nm	Pulsed laser
Energy Position Response	γ - 6.13 MeV	^{16}N
Energy Scale	γ - 6.13 MeV	^{16}N
	γ - 19.8 MeV	$^{3}He(p,\gamma)^{4}He$
	γ - 6.25 MeV	d(n,γ) with n from ^{252}Cf
	β - 13 MeV endpoint	^{8}Li
Neutron Efficiency	n	^{252}Cf, Am-Be
$\beta-\gamma$ background	β,γ	U/Th(^{214}Bi, ^{208}Tl)
Gain Stability	γ - 6.13 MeV	^{16}N

is ≈16 cm and the angular resolution is ≈26.7 degrees.

3. Background Determination

Background neutrons can result from photodisintegration of the deuterons by γs with energy $\geq$ 2.2 MeV. It is therefore very important to measure the actual Th and U radioactivity level in the D_2O and H_2O volume. This was done by applying *ex situ* assay techniques as well as by analyzing the *in situ* Cherenkov light produced. The results from these two methods are consistent with each other (Figs. 3(a) and 3(b).) The external backgrounds are measured by fitting the radial distribution of the data at the AV region with probability distribution functions (pdfs) constructed from β-γ calibration source data. Figs. 4 shows the fitted results for external background with energy above 4.5 MeV. There is a combined 78±12 neutron and 45^{+18}_{-12} Cherenkov background events found in the final data set.

4. Extracting the CC, NC, and ES signal

The data reported here were recorded between Nov. 2, 1999 and May 28, 2001 and represent a total of 306.4 live days of the pure D_2O phase. The data have been analyzed using the same data reduction procedures described in [4], with the addition of a new neutron background cut, yielding 2928 events in the energy region selected for analysis (5 to 20 MeV). Fig. 5 shows the distribution of selected events (for an analysis threshold of $T_{\rm eff}\geq$ 5 MeV and fiducial volume selection of $R \leq 550$ cm, where R is the reconstructed event radius) in (a) $\cos\theta_{\odot}$, (b)volume-weighted radial variable $(R/R_{\rm AV})^3$, where $R_{\rm AV}$ = 600 cm is the radius of the acrylic vessel. Fig. 5(c) shows the kinetic energy spectrum of the selected events.

4.1. Method and Uncertainties

The signal extraction method takes advantage of the very distinct shapes of the CC, NC, and ES interactions in the energy, weighted volume, and sun direction distributions to perform a maximum likelihood fit to decompose the data into the 3 basic components + background. The pdfs in T_{eff}, $\cos\theta_{\odot}$, and $(R/R_{\rm AV})^3$ are derived from Monte Carlo

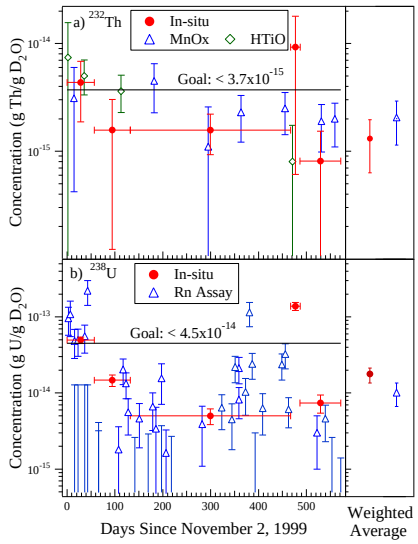

Figure 3. Thorium (a) and uranium (b) backgrounds (equivalent equilibrium concentrations) in the D_2O deduced by *in situ* and *ex situ* techniques. The results are consistent and exceed design goals

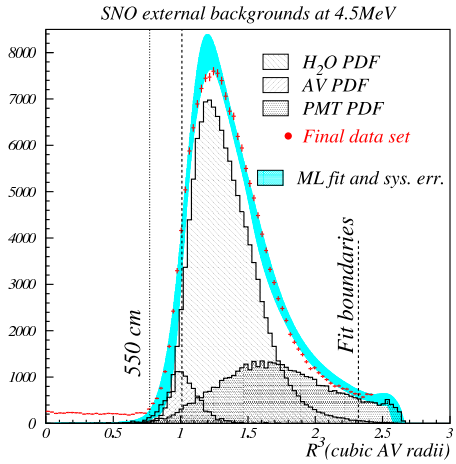

Figure 4. The radial distribution of events from external backgrounds with reconstructed energy above 4.5 MeV. The background pdfs are fixed when performing signal extraction.

calculations assuming no flavor transformation and the standard ^{8}B spectral shape [6]. Background pdfs with fixed amplitudes are also included in the procedure. The signal extraction procedure yields 1968 CC, 264 ES and 577 NC events. The combined experimental systematic uncertainties on fluxes derived by repeating the signal decomposition with perturbed pdfs (constrained by calibration data) is found to be (-5.2, +5.2), (-8.5,+9.1), (-13.2,+14.1) percent for the CC, NC, and $\phi_{\mu,\tau}$ components respectively.

4.2. Results

Normalized to the integrated rates above the kinetic energy threshold of $T_{\rm eff} \geq 5$ MeV, the flux of ^{8}B neutrinos measured with each reaction in SNO, assuming the standard spectrum shape [6] is (all fluxes are presented in units of 10^6 cm^{-2}s^{-1}):

$$\begin{aligned}
\phi_{CC}^{SNO} &= 1.76^{+0.06}_{-0.05}(\text{stat.})^{+0.09}_{-0.09}\ (\text{syst.}) \\
\phi_{ES}^{SNO} &= 2.39^{+0.24}_{-0.23}(\text{stat.})^{+0.12}_{-0.12}\ (\text{syst.}) \\
\phi_{NC}^{SNO} &= 5.09^{+0.44}_{-0.43}(\text{stat.})^{+0.46}_{-0.43}\ (\text{syst.}).
\end{aligned}$$

It can be seen that ϕ_{CC}^{SNO} is *significantly* less than ϕ_{NC}^{SNO}. It is interesting to view the above results in the more convenient neutrino flavor coordinates [4] as shown in Figure 6 ($\phi_{CC} = \phi_e$, $\phi_{ES} = \phi_e + \epsilon\phi_{\mu\tau}$, where ϵ=0.154) :

$$\begin{aligned}
\phi_e &= 1.76^{+0.05}_{-0.05}(\text{stat.})^{+0.09}_{-0.09}\ (\text{syst.}) \\
\phi_{\mu\tau} &= 3.41^{+0.45}_{-0.45}(\text{stat.})^{+0.48}_{-0.45}\ (\text{syst.})
\end{aligned}$$

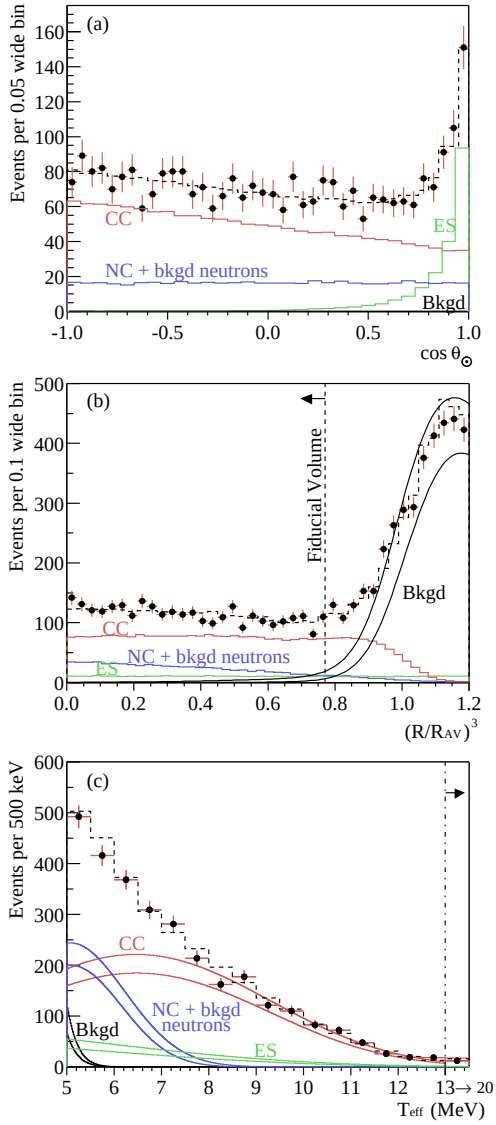

Figure 5. (a) Distribution of $\cos\theta_\odot$ for $R \leq 550$ cm. (b) Distribution of the volume weighted radial variable $(R/R_{\rm AV})^3$. (c) Kinetic energy for $R \leq 550$ cm. Also shown are the Monte Carlo predictions for CC, ES and NC + bkgd neutron events scaled to the fit results, and the calculated spectrum of Cherenkov background (Bkgd) events. The dashed lines represent the summed components, and the bands show $\pm 1\sigma$ uncertainties. All distributions are for events with $T_{\rm eff} \geq 5$ MeV.

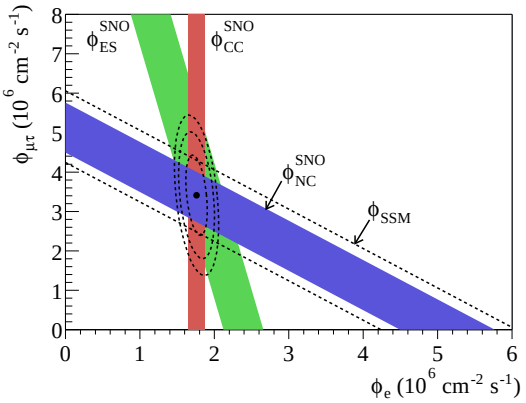

Figure 6. Flux of ^{8}B solar neutrinos which are μ or τ flavor vs flux of electron neutrinos deduced from the three neutrino reactions in SNO. The diagonal bands show the total ^{8}B flux as predicted by the SSM [5] (dashed lines) and that measured with the NC reaction in SNO (solid band). The intercepts of these bands with the axes represent the $\pm 1\sigma$ errors. The bands intersect at the fit values for ϕ_e and $\phi_{\mu\tau}$, indicating that the combined flux results are consistent with neutrino flavor transformation assuming no distortion in the ^{8}B neutrino energy spectrum.

By combining the statistical and systematic uncertainties in quadrature, $\phi_{\mu\tau}$ is $3.41^{+0.66}_{-0.64}$, which is 5.3σ above zero, providing strong evidence for flavor transformation consistent with neutrino oscillations [7,8], which also implies that neutrinos have non-degenerate and finite masses. Figure 6 shows the flux of non-electron flavor active neutrinos vs the flux of electron neutrinos deduced from the SNO data. The three bands represent the one standard deviation measurements of the CC, ES, and NC rates. The error ellipses represent the 68%, 95%, and 99% joint probability contours for ϕ_e and $\phi_{\mu\tau}$.

4.3. Evidence for solar neutrino flavor transformation

In short, SNO has performed the first direct measurement of the total flux of active ^{8}B neutrinos arriving from the sun and provides strong model independent evidence (5.3σ) for neutrino flavor transformation.

5. CC, NC, and ES Day/Night Asymmetry Analysis

The unique multi-flavor capability of SNO can be exploited to study the day-night asymmetry of the CC, NC, and ES fluxes separately for the first time. For certain neutrino oscillation parameters one expect to see an asymmetry in the D versus N rate. The procedure for this study is very similar to the combined analysis except that the systematics need to be considered separately for the day and night data sets in detail. To make sure that no significant asymmetries were introduced from instrumentation and other operational causes, similar day/night ratios for other known event classes were examined. These include electronic pulser signals, muons, spallation neutrons, and known fixed low-level radioactivity spots in the detector, etc. Finally, checks were also made by dividing the data into subclasses such as east versus west with respect to the direction of the sun instead of day versus night. There are no significant bias observed from these studies. Similar to the combined case, one can perform signal extraction on the data and form new day-night ratios from the corresponding extracted ϕ_N and ϕ_D fluxes:

$$\mathcal{A}_\alpha = 2(\phi_N^\alpha - {\phi_D}^\alpha)/(\phi_N^\alpha + {\phi_D}^\alpha) where \alpha = CC, NC, ES \quad (2)$$

The day and night energy spectra for all accepted events are shown in the upper part of Fig. 7. Backgrounds were subtracted separately for day and night as part of the signal extraction. The results were normalized for an Earth-Sun distance of 1 AU, yielding the results in Table 3.

Table 3
The results of D/N signal extraction by assuming an undistorted ^{8}B spectrum. $\mathcal{A}$ is the asymmetry parameter. The systematic uncertainties (combined set) include a component that cancels in the formation of the $\mathcal{A}$. Except for the dimensionless $\mathcal{A}$, the units are 10^6 cm^{-2} s^{-1}.

signal	ϕ_D	ϕ_N	$\mathcal{A}(\%)$
CC	$1.62 \pm 0.08 \pm 0.08$	$1.87 \pm 0.07 \pm 0.10$	$+14.0 \pm 6.3^{+1.5}_{-1.4}$
ES	$2.64 \pm 0.37 \pm 0.12$	$2.22 \pm 0.30 \pm 0.12$	$-17.4 \pm 19.5^{+2.4}_{-2.2}$
NC	$5.69 \pm 0.66 \pm 0.44$	$4.63 \pm 0.57 \pm 0.44$	$-20.4 \pm 16.9^{+2.4}_{-2.5}$

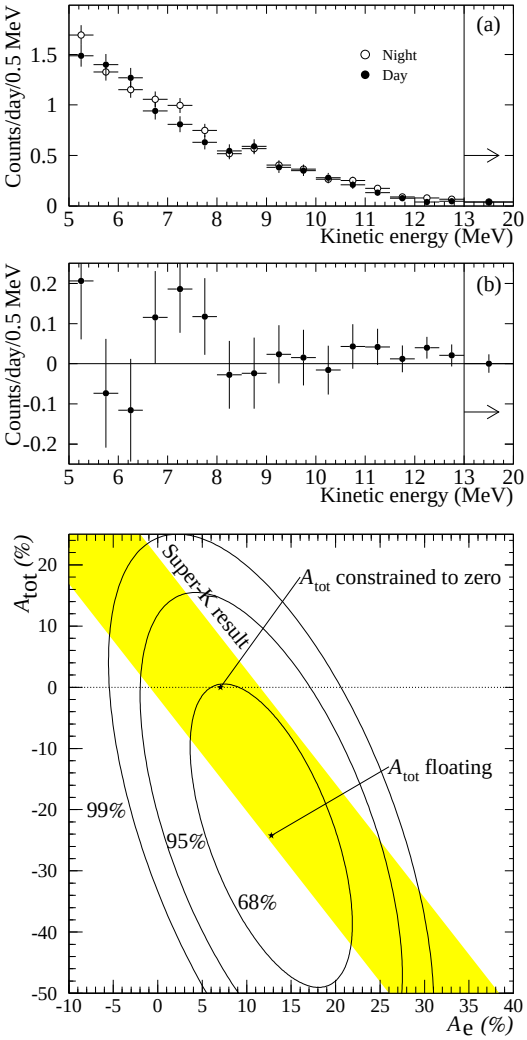

Figure 7. Upper: (a) Energy spectra for day and night. All signals and backgrounds contribute. The final bin extends from 13.0 to 20.0 MeV. (b) Difference, *night - day*, between the spectra. The day rate was 9.23 ± 0.27 events/day, and the night rate was 9.79 ± 0.24 events/day. Lower: Joint probability contours for $\mathcal{A}_{tot}$ and $\mathcal{A}_e$. The points indicate the results when $\mathcal{A}_{tot}$ is allowed to float and when it is constrained to zero. The diagonal band indicates the 68% joint contour for the Super-K $\mathcal{A}_{ES}$ measurement.

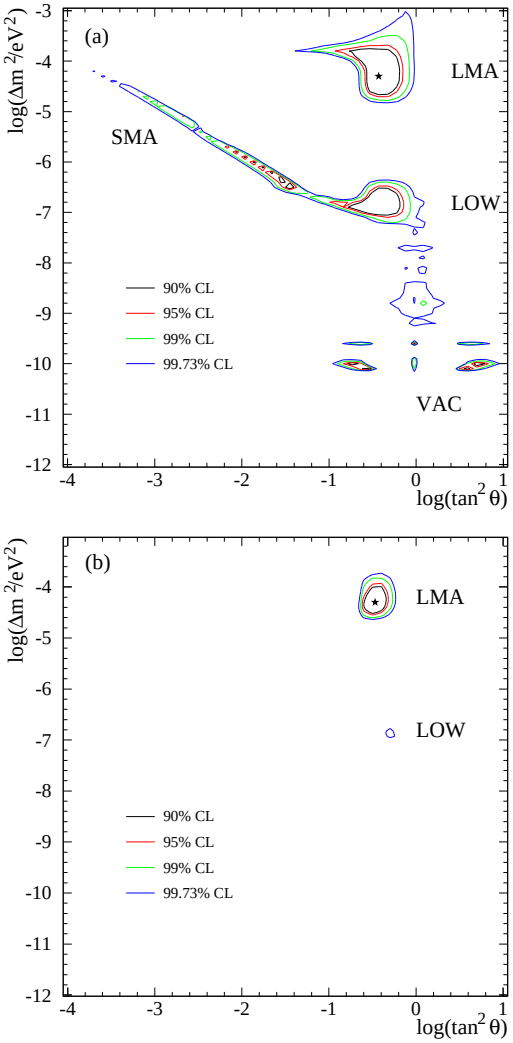

Figure 8. Upper; Allowed regions of the MSW plane determined by a χ^2 fit to SNO day and night energy spectra. Lower: by a χ^2 fit to SNO day and night energy spectra with additional experimental and solar model data.The star indicates the best fit. See text for details.

Note that these are direct signal extraction results with the CC, NC, and ES components are treated independently except for the correlations adhered from the numerical extraction procedure. One can impose further constraints to the above results by the fact that ES is a mixture of both CC and NC processes. Another approach is to require that $\mathcal{A}_{tot}$=0. The latter case is shown in the lower portion of Figure 7. By forcing $\mathcal{A}_{tot} = 0$, as predicted by active-only models, $\mathcal{A}_e = 7.0\% \pm 4.9\%$ (stat.)$^{+1.3}_{-1.2}\%$ (sys.).

6. Neutrino Oscillations and MSW parameters

SNO's day and night energy spectra (Fig. 7) have also been used to produce MSW exclusion plots and limits on neutrino flavor mixing parameters. MSW oscillation models between two active flavors were fit to the data. For simplicity, only the energy spectra were used in the fit, and the radial R and direction $\cos\theta_\odot$ information was omitted. This procedure preserves most of the ability to discriminate between oscillation solutions. A model was constructed for the expected number of counts in each energy bin by combining the neutrino spectrum [6], the survival probability, and the cross sections [9] with SNO's response functions [10].

There are 3 free parameters in the fit: the total ^{8}B flux ϕ_B, the difference Δm^2 between the squared masses of the two neutrino mass eigenstates, and the mixing angle θ. The flux of higher energy neutrinos from the solar *hep* reaction was fixed at 9.3×10^3 cm^{-2} s^{-1} [16]. Contours were generated in Δm^2 and $\tan^2\theta$ for $\Delta\chi^2(c.l.) = 4.61\ (90\%), 5.99\ (95\%), 9.21\ (99\%)$, and 11.83 (99.73%). Fig. 8(a) shows allowed mixing parameter regions using only SNO data with no additional experimental constraints or inputs from solar models. By including flux information from the Cl [17] and Ga experiments [12–15], the day and night spectra from the SK experiment [11], along with solar model predictions for the more robust *pp*, *pep* and ^{7}Be neutrino fluxes [16], the contours shown in Fig. 8(b) were produced. This global analysis strongly favors the Large Mixing Angle (LMA) region (see Table 4), and $\tan^2\theta$ values < 1. Repeating the global analysis using the total SNO energy spectrum instead of separate day and night spectra gives nearly identical results.

Table 4
Best fit points in the MSW plane for global MSW analysis using all solar neutrino data. ϕ_B is the best-fit ^{8}B flux for each point, and has units of 10^6 cm^{-2} s^{-1}. Δm^2 has units of eV^2. $\mathcal{A}_e$ is the predicted asymmetry for each point.

Region	χ^2_{min}/dof	ϕ_B	$\mathcal{A}_e$(%)	Δm^2	$\tan^2\theta$	c.l.(%)
LMA	57.0/72	5.86	6.4	5.0×10^{-5}	0.34	—
LOW	67.7/72	4.95	5.9	1.3×10^{-7}	0.55	99.5

7. Summary

The results presented here are the first direct measurement of the total flux of active ^{8}B neutrinos arriving from the sun and provide strong evidence for neutrino flavor transfor-

mation. Specifically, we have empirically established that there is a non-ν_e component in the solar neutrino flux, with $\phi_{\mu\tau} = 3.41^{+0.45}_{-0.45}(\text{stat.})^{+0.48}_{-0.45}$ (syst.) $\times 10^6$ cm^{-2}s^{-1}, 5.3σ greater than zero. The total flux of ^{8}B neutrinos measured with the NC reaction is in agreement with the SSM prediction. By constraining the D/N asymmetry of the total active flux to zero, the asymmetry for the ν_e flux is $\mathcal{A}_e = 7.0\% \pm 4.9\%$ (stat.)$^{+1.3}_{-1.2}\%$ (sys.). A global fit to SNO's day and night energy spectra and data from other solar neutrino experiments strongly favors the LMA solution in a 2-flavor MSW neutirno oscillation analysis.

This research was supported by: Canada: NSERC, Industry Canada, NRC, Northern Ontario Heritage Fund Corporation, Inco, AECL, Ontario Power Generation; US: Dept. of Energy; UK: PPARC. We thank the SNO technical staff for their strong contributions.

REFERENCES

1. The SNO Collaboration
.5 Q.R. Ahmad, R.C. Allen, T.C. Andersen, J.D. Anglin, G. Bühler, J.C. Barton, E.W. Beier, M. Bercovitch, J. Bigu, S. Biller, R.A. Black, I. Blevis, R.J. Boardman, J. Boger, E. Bonvin, M.G. Boulay, M.G. Bowler, T.J. Bowles, S.J. Brice, M.C. Browne, T.V. Bullard, T.H. Burritt, K. Cameron, J. Cameron, Y.D. Chan, M. Chen, H.H. Chen X. Chen, M.C. Chon, B.T. Cleveland, E.T.H. Clifford, J.H.M. Cowan, D.F. Cowen, G.A. Cox, Y. Dai, X. Dai, F. Dalnoki-Veress, W.F. Davidson, P.J. Doe, G. Doucas, M.R. Dragowsky, C.A. Duba, F.A. Duncan, J. Dunmore, E.D. Earle, S.R. Elliott, H.C. Evans, G.T. Ewan, J. Farine, H. Fergani, A.P. Ferraris, R.J. Ford, M.M. Fowler, K. Frame, E.D. Frank, W. Frati, J.V. Germani, S. Gil, A. Goldschmidt, D.R. Grant, R.L. Hahn, A.L. Hallin, E.D. Hallman, A. Hamer, A.A. Hamian, R.U. Haq, C.K. Hargrove, P.J. Harvey, R. Hazama, R. Heaton, K.M. Heeger, W.J. Heintzelman, J. Heise, R.L. Helmer J.D. Hepburn, H. Heron, J. Hewett, A. Hime, M. Howe, J.G. Hykawy, M.C.P. Isaac, P. Jagam, N.A. Jelley, C. Jillings, G. Jonkmans, J. Karn, P.T. Keener, K. Kirch, J.R. Klein, A.B. Knox, R.J. Komar, R. Kouzes, T. Kutter, C.C.M. Kyba, J. Law, I.T. Lawson, M. Lay, H.W. Lee, K.T. Lesko, J.R. Leslie, I. Levine, W. Locke, M.M. Lowry, S. Luoma, J. Lyon, S. Majerus, H.B. Mak, A.D. Marino, N. McCauley, A.B. McDonald, D.S. McDonald, K. McFarlane, G. McGregor, W. McLatchie, R. Meijer Drees, H. Mes, C. Mifflin, G.G. Miller, G. Milton, B.A. Moffat, M. Moorhead, C.W. Nally, M.S. Neubauer, F.M. Newcomer, H.S. Ng, A.J. Noble E.B. Norman, V.M. Novikov, M. O'Neill, C.E. Okada, R.W. Ollerhead, M. Omori, J.L. Orrell, S.M. Oser, A.W.P. Poon, T.J. Radcliffe, A. Roberge, B.C. Robertson, R.G.H. Robertson, J.K. Rowley, V.L. Rusu, E. Saettler, K.K. Schaffer, A. Schuelke, M.H. Schwendener, H. Seifert, M. Shatkay, J.J. Simpson, D. Sinclair, P. Skensved, A.R. Smith, M.W.E. Smith, N. Starinsky, T.D. Steiger, R.G. Stokstad, R.S. Storey B. Sur, R. Tafirout, N. Tagg, N.W. Tanner, R.K. Taplin, M. Thorman, P. Thornewell, P.T. Trent Y.I. Tserkovnyak, R. Van Berg, R.G. Van de Water, C.J. Virtue, C.E. Waltham, J.-X. Wang, D.L. Wark, N. West, J.B. Wilhelmy, J.F. Wilkerson, J. Wilson, P. Wittich, J.M. Wouters, M. Yeh
2. The SNO Collaboration, Nucl. Instr. and Meth. **A449**, 172 (2000).
3. H. Chen, Phys.Rev.Lett. (1984)
4. Q.R. Ahmad *et al.*, Phys. Rev. Lett. **87**, 071301 (2001)
5. J.N. Bahcall, M.H. Pinsonneault, and S. Basu, Astrophys. J. **555**, 990 (2001)
6. C.E. Ortiz *et al.*, Phys. Rev. Lett. **85**, 2909 (200)
7. Z. Maki, N. Nakagawa, and S. Sakata, Prog. Theor. Phys. **28**, 870 (1962)
8. B.M. Pontecorvo, V.N. Gribov, Phys. Lett. B **28**, 493 (1969)
9. S. Nakamura *et al.*, (2002), nucl-th/0201062.
10. http://sno.phy.queensu.ca
11. S. Fukuda *et al.*, Phys. Rev. Lett. **86**, 5651 (2001).
12. J.N. Abdurashitov *et al.*, Phys. Rev. C **60**, 055801, (1999).
13. M. Altmann *et al.*, Phys. Lett. B **490**, 16 (2000).
14. W. Hampel *et al.*, Phys. Lett. B **447**, 127 (1999).
15. C.M. Cattadori *et al.*, in *Proceedings of the TAUP 2001 Workshop*, (September 2001), Assergi, Italy.
16. From www.sns.ias.edu/ jnb. Also see J.N. Bahcall, M. H. Pinsonneault, and S. Basu, astro-ph/0010346 v2.
17. B.T. Cleveland *et al.*, Astrophys. J. **496**, 505 (1998).